AN INVESTIGATION OF A RADIAL DIFFUSER USING INCOMPRESSIBLE FLOW WITHOUT SWIRL

by

Paul S. Moller

Report 63-9

Mechanical Engineering Research Laboratories

McGill University

Supported under D.R.B. Grant Number 9551-12

Montreal July 1963

ACKNOWLEDGEMENTS

The author wishes to thank Dr. B.G. Newman for his valuable suggestions and criticisms in the course of this work.

Messrs. A. Gustavsen and E. Hansen are thanked for their assistance in the construction of the apparatus.

The work was financially supported by the Defence Research Board of Canada under D.R.B. Grant Number 9551-12.

SUMMARY

Due to the geometric limitations of certain internal flow systems, the use of a conical or rectangular diffuser for energy conversion is often impossible. This paper describes a study of swirl-free, incompressible flow in a radial diffuser consisting of two components: a radial channel in which the flow diffusion occurs and an inlet bend which joins the radial channel to the supply pipe outlet.

A design for an efficient inlet bend is described and a study made of certain other geometrical parameters. The experiments showed that the pressure recovery decreased with increasing inlet boundary layer thickness and decreasing Reynolds number, both for the radial diffuser and a 7^{o} conical diffuser of the same area ratio. In addition, the pressure recovery of the radial diffuser was comparable to that of the 7^{o} conical diffuser at the high Reynolds numbers generally encountered in internal flow systems. At high Reynolds numbers it was also possible to predict theoretically the pressure recovery for the radial diffuser.

CONTENTS

NOTATION

Roman Symbols

A - area

C_f - friction coefficient $\frac{\tau_w}{\frac{1}{2}\rho\bar{U}^2}$

C_{p_R} - pressure recovery coefficient $\frac{p_e - p_i}{\frac{1}{2}\rho\bar{U}^2}$

D - channel diameter

d - inlet pipe diameter

h - channel height or width

h_b - distance between centre-body and outer wall of bend measured along perpendicular to the outer wall

n - power-law exponent describing the turbulent velocity profile

Δp_b - total pressure loss in the inlet bend

Δp_{ch} - total pressure loss due to friction in the radial channel

p - static pressure on the channel wall and outer wall of the bend (time mean when turbulent)

p_o - stagnation pressure $r = 0$, $z = 0$

p_∞ - static-pressure of surrounding fluid at rest

q - dynamic pressure

Q - volume flow

r - radial cylindrical co-ordinate measured from the centre-line of the inlet pipe

R - radius of curvature of outer wall in the inlet bend

R_e - channel Reynolds number based on the mean velocity and twice the channel width $\frac{\bar{u}2h}{\nu}$

R_d - inlet pipe Reynolds number $\frac{\bar{U}d}{\nu}$

$\bar{U}$ - space mean velocity in the inlet pipe

u - time mean velocity in the radial direction or along the inlet pipe

$\bar{u}$ - space mean velocity in the radial channel

U_∞ - velocity outside the boundary layer for flow over a flat plate

U_c - maximum mean velocity at the centre of inlet pipe

U_o - local maximum mean velocity in the centre of the channel

w - mean velocity in the axial direction

x - distance measured along bend wall downstream of bend inlet

z - axial co-ordinate measured perpendicular to the channel wall downstream of the pipe inlet

Greek Symbols:

θ - angle of bend measured downstream of bend inlet

ρ - density of fluid

δ - boundary layer thickness

δ^* - displacement thickness of boundary layer

ν - kinematic viscosity of fluid

τ_w - wall shear stress or skin friction

Subscripts:

c - centre-body

e - at diffuser exit

i - at diffuser inlet

o - outer-wall of inlet bend (Figure 2)

1. INTRODUCTION

The object of this investigation was to determine the geometrical and flow parameters which are important in the design of an efficient, incompressible-flow, radial diffuser. Experimental and theoretical studies carried out by the author in a previous analysis[1] have lead to the accurate prediction of the pressure losses due to friction in turbulent radial channel flow. This information makes it possible to predict the pressure recovery for a purely radial diffusing section. One of the chief difficulties in the application of this configuration as an efficient diffuser is the problem of turning the flow from the supply pipe outlet to the radial channel inlet. This must be accomplished with a very small pressure loss if a radial diffuser is to be competitive with a conical diffuser of the same area ratio. Since it is desirable to prevent flow separation from the boundaries of this bend, little or no diffusion can take place there. The channel width is therefore directly linked to the important bend loss parameter, the mean radius ratio (defined as the ratio of the local mean radius of the bend to the local width of the bend). As the channel width increases, the channel pressure losses will decrease, but the bend losses may increase due to a decrease in the mean radius ratio.

Little is known about bend losses in simple situations, let alone in the case where the radius ratio is changing throughout a three dimensional bend. Hofmann[2]

has made an extensive experimental study of diffusers in which some of the configurations tested were similar to that of radial flow between parallel discs. The highest pressure recovery $(\frac{\bar{p}_{exit} - \bar{p}_{in}}{\bar{q}_{in}})$ achieved was 0.72. However, by making the supply pipe into a short wide-angle conical diffuser (total included angle of expansion = 17°) and then following it by a radial diffuser, a pressure recovery of 0.86 was achieved. Very little of the actual flow diffusion took place in the radial channel, however, since it was very short.

The effect of Reynolds number on pressure recovery has not been investigated in any great detail. Kline et al[3] have suggested that the pressure recovery may decrease with Reynolds number, and the experiments of Robertson and Ross,[4] with conical diffusers using water, have shown a slight decrease in pressure recovery with Reynolds number. It might be expected that the effects of Reynolds number on pressure recovery will be due mainly to friction in the radial diffuser since the channel exit velocity profile will generally be fully developed. However, in the conical diffuser, changes in the pressure recovery due to Reynolds number will probably be the result of altering the transitory stall (turbulent level) and the exit kinetic energy losses, i.e., the losses associated with having a highly non-uniform velocity profile at the exit.

A second flow parameter that influences the pressure recovery is the boundary layer thickness at the inlet to the diffuser. A number of investigations[4, 5, 6] have shown that pressure recovery decreases with increased boundary layer

thickness at the inlet; the decrease is greatest when the diffusion takes place most rapidly, i.e., conical diffusers with large inclined angles of expansion.

In the present investigation, an efficient channel inlet is developed by approximating the experimental results of Reich[7] for the free streamlines of an impinging axi-symmetric jet. In addition, the effects of Reynolds number, inlet boundary layer thickness, and the inclusion of a centre-body are determined experimentally. The pressure recovery is predicted theoretically by assuming that the flow is not separated from the bend walls and that the inlet boundary layers are negligibly thin. The experimental results for the pressure recovery in the radial diffuser are compared with those for a 7° conical diffuser.

2. THEORY

2.1 Design of the Radial-Channel Inlet Bend

If the flow were to negotiate the 90° inlet bend in a frictionless manner with a constant pressure on the outer wall, the situation would be similar to that of an impinging axisymmetric jet on a flat plate when the jet does not mix with the surrounding fluid. The effects of friction in altering this model are unknown, but in order to provide a basis from which to develop an efficient inlet contour, the free streamline boundaries for such a model were examined. In Figure 1, the experimental results of Reich[7] are shown together with the theoretical calculations of Schacht[8] for an axisymmetric water jet impinging on a flat plate at right angles to the direction of flow. The initial part of the experimental curve can be approximated quite well by a circular-arc of radius $R = 0.375d$, and thus the boundary shape has the merit of being easy to define and to manufacture. With this design, the areas of the supply pipe outlet and the channel inlet are equal. In this condition a slight pressure drop would be expected in the bend due to boundary layer growth. The radius R is kept as small as a circular-arc approximation to the experimental results will allow so that, with the same area at the bend inlet and exit, the channel width will be as large as possible and the overall size of the radial channel minimized for a given area ratio $\frac{A_e}{A_i}$.

2.2 Design of a Centre-Body

The effect of a centre-body or corner-body on bend losses is the subject of some controversy. Although it helps to prevent separation, it also increases friction losses. McLellan and Bartlett[9] have found an increased pressure loss by filling in the outside corner of a 90° square bend. However, this finding is contrary to the results of Wirt[10], who found a reduced pressure loss for nearly the same geometry. A centre-body was therefore designed for the present case in order that its influence on the flow could be determined. The contour for the centre-body was chosen so that with one-dimensional flow, the bend area was kept constant. Thus the centre-body contour could be evaluated by means of the following formula, which gives the distances between the inlet boundary 0 - 0 and the centre-body contour c - c as measured along perpendiculars to the inlet boundary (Figure 2):

$$\frac{h_b}{d} = (0.875 \sec\theta - 0.375) - \left[(0.875 \sec\theta - 0.375)^2 - \frac{\sec\theta}{4}\right]^{\frac{1}{2}} \quad \ldots(1)$$

Since the diameter of the inlet pipe is usually fixed, this has been chosen as the most suitable length for non-dimensionalizing the other length parameters.

2.3 Pressure Losses in the Inlet Bend

It has been shown (Moller [1]) that the critical Reynolds number for reverse transition for radial flow between parallel discs is approximately 2000. Therefore, laminar flow will exist at the radial diffuser exit if $3.5\ R_d(\frac{A_e}{A_i}) < 2000$. If the critical Reynolds number for reverse transition in conical diffusers is assumed to be 2000 or less, the flow will be turbulent at the conical diffuser exit when $R_d \cdot \frac{A_e}{A_i} > 2000$. In general, however, the operational Reynolds numbers in both conical and radial diffusers will be considerably greater than these limiting values. Therefore the flow is usually turbulent throughout the channel.

Previous investigations into bend losses with turbulent flow [11, 12, 13] have been primarily concerned with the increased pressure losses due to secondary flow associated with the bend. Secondary flows are unlikely in the present case because of the radial symmetry. However, if flow separation were to occur, secondary flows in the z - r plane would result.

The following assumptions are made to facilitate a theoretical prediction of the pressure losses in the bend.

1. The flow is assumed to be one-dimensional throughout the bend:
   a) the flow is not separated from the walls
   b) the boundary layers are gegligibly thin at the supply pipe outlet and throughout the bend.

2. The skin friction is taken from experimental results for a growing turbulent boundary layer on a flat plate:

   a) The region of laminar flow that might be expected to exist near the stagnation point on the centre body is neglected.

   b) The increase of velocity associated with the blockage effect of the boundary layers has a negligible effect on the skin friction.

   c) The effects of the pressure gradients on the skin friction are selfcompensating e.g. on the wall 0 - 0 the friction coefficient constant in equ. (3) below (0.0570) is too high in the adverse pressure gradient while the dynamic pressure used in defining the skin friction coefficient is usually too low.

For the model shown in Figure 2, the momentum integral equation is:

$$dp = 8 \left\{ \frac{r_c}{d}\left(0.375 + \frac{h_b}{d}\right) \tau_{w_c} + \frac{r_o}{d}\ 0.375\ \tau_{w_o} \right\}\ d\theta \qquad \ldots(2)$$

The wall shear stress τ_w is taken from Schlichting [14] for turbulent boundary layers on a flat plate.

$$c_f = \frac{\tau_w}{\frac{1}{2}\rho \bar{U}_\infty^2} = \frac{0.0576}{\left(\frac{U_\infty x}{\nu}\right)^{1/5}}$$

For thin boundary layers on the bend walls (displacement effects neglected), this can be written

$$C_f = \frac{\tau_w}{\frac{1}{2}\rho\bar{U}^2} = \frac{0.0576}{\left(\frac{\bar{U}x}{\nu}\right)^{1/5}} \qquad \ldots(3)$$

where x is measured along the bend wall and $\bar{U}$ is the mean velocity in the bend. Alternatively a constant skin friction coefficient might have been used. However, in this case increasing the diffuser size and hence the Reynolds number would not lead to a reduced skin friction. Since a scale factor of 10 may be involved, a skin friction coefficient including Reynolds number gives a somewhat more useful result.

Substituting for τ_o and r and integrating from the supply pipe exit ($\theta = 0^o$) to the radial channel inlet ($\theta = 90^o$), equation (2) becomes:

$$\frac{\Delta p_b}{\frac{1}{2}\rho\bar{U}^2} = -\frac{.4608}{(R_d)^{1/5}} \int_{\theta=0^o}^{\theta=90^o} \left[\frac{0.875(0.375 + \frac{h_b}{d}) - (0.375 + \frac{h_b}{d})^2 \cos\theta}{(\frac{x_c}{d})^{1/5}} + \frac{0.875(0.375) - (0.375)^2 \cos\theta}{(\frac{x_o}{d})^{1/5}} \right] d\theta$$

where $\frac{h_b}{d}$ is given by equation (1)

and Δp_b is the pressure loss in the bend due to friction. Integrating the R.H.S. of the above equation graphically gives:

$$\frac{\Delta p_b}{\frac{1}{2}\rho\bar{U}^2} = \frac{0.3875}{(R_d)^{1/5}} \qquad \ldots(4)$$

2.4 Radial Diffuser Pressure Recovery

The usefulness of a diffuser is usually assessed in terms of its static pressure recovery, or the ratio of the static pressure rise to the input dynamic pressure. Since the pressure may not be uniform at the diffuser inlet and exit, the pressure recovery coefficient is usually chosen as:

$$C_{P_R} = \frac{\frac{1}{A_e}\int_{A_e} p_e dA_e - \frac{1}{A_i}\int_{A_i} p_i dA_i}{\frac{1}{A_i}\int_{A_i} q_i dA_i} \qquad \ldots(5)$$

where subscripts i and e refer to inlet and exit conditions respectively. A more meaningful average for the dynamic pressure would be the energy average $\frac{1}{A_i \bar{U}}\int_{A_i} q_i U dA_i$, however this is not generally used.

With a boundary layer at the supply pipe outlet, the ratio of the mean dynamic pressure of the flow to the dynamic pressure of the mean velocity is:

$$\frac{q_i}{\frac{1}{2}\rho\bar{U}^2} = \frac{\left(1 - \frac{\delta}{d/2}\right)^2}{\left(1 - \frac{\delta^*}{d/2}\right)^2} + \frac{1}{\bar{U}^2}\int_{\left(1 - \frac{\delta}{d/2}\right)}^{1} u^2 \left(\frac{r}{d/2}\right) d\left(\frac{r}{d/2}\right)$$

where δ^* is the annular thickness or mean velocity which equals the deficit of volume flow in the boundary layer, and δ is the thickness of the boundary layer at the pipe exit. Representing the velocity profile by a power-law and considering the extreme case where the boundary layer is fully developed ($\delta = d/2$), the actual dynamic pressure is approximately 2% higher than the one-dimensional dynamic pressure. Therefore

this difference is, in general, very small for ($\delta < d/2$), and the dynamic pressure may be evaluated from measurement of the mean velocity in the pipe. The same argument can be applied at the radial channel exit where the flow will be fully developed ($\delta = h/2$).

Thus

$$\frac{q_e}{\frac{1}{2}\rho\bar{u}_e^2} = \frac{(n+1)^2}{n(2+n)} \qquad \ldots(6)$$

and in this case the difference between the actual dynamic pressure and the one-dimensional dynamic pressure is even less than for pipe flow with a fully developed velocity profile ($n = 7$). Furthermore the slight errors introduced into the calculation of q_e and q_i by using the one-dimensional dynamic pressure tend to cancel each other.

Assuming that the static pressure is constant across both the supply pipe outlet and the radial channel exit, equation (5) becomes:

$$c_{p_R} = \frac{p_e - p_i}{\frac{1}{2}\rho\bar{u}^2} \qquad \ldots(7)$$

The solution for the radial pressure distribution is carried over from a previous analysis (Moller[1]).

$$\frac{p-p_\infty}{\frac{1}{2}\rho Q^2} h^4 = -\frac{16}{63\pi^2}\left(\frac{h}{D}\right)^2\left(\left(\frac{D}{r}\right)^2 - 4\right) + 0.007089\left(\frac{h}{D}\right)^{\frac{3}{4}}\left(\frac{h\nu}{Q}\right)^{\frac{1}{4}}\left(\left(\frac{D}{r}\right)^{\frac{3}{4}} - 1.682\right)$$

Non-dimensionalizing this equation with respect to the supply

pipe diameter and the one-dimensional dynamic pressure gives, for $\frac{h}{d} = 0.143$,

$$\frac{p-p_\infty}{\frac{1}{2}\rho\bar{U}^2} = -0.778\left[\left(\frac{1}{r/d}\right)^2-\left(\frac{2}{D/d}\right)^2\right]+\frac{1.590}{(R_d)^{1/4}}\left[\left(\frac{1}{r/d}\right)^{\frac{3}{4}}-\left(\frac{2}{D/d}\right)^{\frac{3}{4}}\right] \quad ...(8)$$

$$\text{where } R_d = \frac{\bar{U}d}{\nu}$$

Extracting the friction pressure loss term from equation (8) and evaluating it at the channel inlet ($\frac{r}{d} = 0.875$), the pressure loss coefficient for the radial channel becomes:

$$\frac{\Delta p_{ch}}{\frac{1}{2}\rho\bar{U}^2} = \frac{2.674}{(R_d)^{1/4}}\left[0.658 - \left(\frac{d}{D}\right)^{\frac{3}{4}}\right] \quad ...(9)$$

Substituting $p_i = p_e + \Delta p_{ch} + \Delta p_b - (q_i - q_e)$ into equation (6), where Δp_{ch}, Δp_b and q_e are given by equations (9), (4) and (6) respectively, and $q_i = \frac{1}{2}\rho\bar{U}^2$, gives

$$C_{p_R} = 1 - 3.11\left(\frac{d}{D}\right)^2 - \frac{2.674}{(R_d)^{1/4}}\left[0.658 - \left(\frac{d}{D}\right)^{\frac{3}{4}}\right] - \frac{0.388}{(R_d)^{1/5}} \quad ...(10)$$

Equation (10) gives the pressure recovery for the radial diffuser with a thin inlet boundary layer. It may be compared with experiment by means of equation (7).

2.5 Optimum Area Ratio

As the exit diameter of the channel increases, the term associated with the loss of kinetic energy at exit will decrease. However the channel frictional losses will increase. Hence there is presumably an optimum value of the area ratio $\frac{A_e}{A_i}$, which gives the maximum pressure recovery.

Differentiating equation (10) with respect to the channel diameter D gives for a maximum:

$$\frac{d}{dD}\left\{-3.11\left(\frac{d}{D}\right)^2 + \frac{2.674}{(R_d)^{1/4}}\left(\frac{d}{D}\right)^{\frac{3}{4}}\right\} = 0$$

which gives:

$$\left(\frac{A_e}{A_i}\right)_{\text{optimum}} = 0.572\left(\frac{D}{d}\right)_{\text{optimum}} = 1.413\, R_d^{\frac{1}{5}} \qquad \ldots(11)$$

Equation (11) indicates that in general, the optimum area ratio will be quite large.

3. DETAILS OF THE EXPERIMENTAL INVESTIGATION

The experimental apparatus which was used to investigate both the radial and the conical diffuser is shown in Figure 13. A comprehensive study was made for turbulent flow and included

1. The relation between Reynolds number Rd and pressure recovery, C_{p_R}, for both radial and conical diffusers,
2. The effects of a thick boundary layer (fully developed pipe flow) at the inlet to the diffusers.

For the radial diffuser only:

3. The effect of using a centre-body in the inlet bend section,
4. The influence on pressure losses of contracting or expanding the flow as it negotiates the inlet bend between the supply pipe exit and the radial channel entrance,
5. The effect of varying the disc diameter and hence area ratio $\frac{A_e}{A_i}$.

The final inlet supply pipe between the bleed valve and the diffuser was made sufficiently long ($\frac{L}{d} > 100$) for swirl-free, fully developed incompressible pipe flow to exist at the diffuser inlet. However, provision was made for the installation of special screens with greater porosity near the pipe wall. This screen was used to flatten the velocity profile and thus simulate thin boundary layers at the inlet to the radial diffuser. Pitot traverses were made of the

velocity profiles across the channel both near the bend exit and farther downstream. In addition, the supply pipe exit was traversed to measure the effectiveness of the screen in reducing the apparent boundary layer thickness.

All measurements were made at effectively incompressible speeds with $\frac{p_o}{p_\infty} < 1.075$.

4. DISCUSSION OF EXPERIMENTAL RESULTS AND COMPARISON WITH THEORY

When a nearly uniform velocity profile at the supply pipe exit was desired, a composite screen with greater porosity near the pipe wall was used. The details of this screen can be found in the Appendix. To determine the symmetry and apparent boundary layer thickness of the flattened velocity profiles, pitot traverses were made at the pipe exit for three Reynolds numbers. Figure 3 shows that the apparent boundary layer thickness has been reduced to approximately 0.04 of the pipe radius.

4.1 Diffuser Pressure Recovery

Figure 4 shows the pressure recovery coefficient C_{P_R} plotted against the inlet supply pipe Reynolds number R_d. The centre-body is in position, and the boundary layer is thin at the pipe exit ($\delta < 0.020d$). The theory for the radial diffuser under these conditions (equation 10) shows good agreement with the experimental results $R_d > 2 \times 10^5$ in which case the pressure recovery becomes nearly independent of Reynolds number ($C_f \approx F(R_d^{1/4})$). Below $R_d = 2 \times 10^5$, the pressure recovery drops off rapidly and quickly falls below the theoretical prediction. The reason for this is not clearly understood. Flow visualization techniques did not indicate separation of the flow within the inlet bend or the radial channel. One possibility is that the lower Reynolds numbers result in a larger boundary layer, particularly on outer wall 0 - 0 with the velocity profile moving more rapidly towards

a separated state on this wall. The resultant increased displacement thickness, and hence flow blockage, causes an increased skin friction on the centre-body and also beyond the bend exit if the large displacement thickness is maintained downstream of the channel inlet. The velocity traverses taken at the bend exit, as shown in Figure 5, tend to support this hypothesis. The experimental results for the conical diffuser are also plotted in Figure 4, and these show a more gradual decrease in pressure recovery with decreasing Reynolds number when compared with the radial diffuser. In the conical diffuser, the frictional losses are generally small. Hence the main pressure losses stem both from the non-uniformity of the velocity profiles, which enhance the loss of kinetic energy at the channel exit, and from the transitory stall which increases the turbulence level. Both of these losses will increase with increasing boundary layer displacement thickness. Also included in Figure 4 is an experimental point from Gibson[15] for a conical diffuser with an included angle of approximately 7.5°. The larger area ratio probably accounts for the slight difference between his result and the present experimental results.

Figure 6 shows that, in general, the pressure recoveries with thick inlet boundary layers ($\delta = \frac{d}{2}$) are considerably lower than those with thin inlet boundary layers ($\delta < 0.020\ d$). Only at very low Reynolds numbers, with the channel flow partly laminar, do the pressure recoveries

coincide for the two cases. The difference in pressure recovery at high Reynolds numbers ($R_d > 2 \times 10^5$) is nearly a constant, the thick inlet boundry layer pressure recoveries being approximately 8% lower. It is interesting to note that the presence of a centre-body does not appreciably affect the pressure recovery. This is a fortunate result since it gives some flexibility in the design of a radial diffuser. The experimental results for the conical diffuser are also shown in Figure 6 for comparison. The trends displayed in Figure 4 for the thin inlet boundry layer case are repeated, with the conical diffuser pressure recovery again slightly higher at high Reynolds number.

Figure 7 shows the velocity traverses at the bend exit for fully developed pipe flow at the diffuser inlet. The displacement of the maximum velocity towards the front disc leads to what is apparently a large velocity gradient and hence skin friction on this surface. However, the shape of the velocity profile at the bend exit is determined by both viscous and inertia forces in the bend. It is therefore difficult to predict the skin friction from the shape of the velocity profile unless very definitive measurements are made of the velocity gradient at the walls. The apparent increased velocity gradient on the front disc with decreasing Reynolds number is consistent with the decrease of pressure recovery with Reynolds number provided that changes in the skin friction on the back disc are less important.

4.2 Pressure Distribution

The effect of the inlet boundary layer thickness on the radial pressure distribution is shown in Figures 8 and 9. It is observed that the local static pressures are lower for some distance downstream of the channel inlet when the inlet boundary layer is fully developed. This result can be explained by examining the coefficient $\frac{(n+1)^2}{n(2+n)}$ which, as shown in equation 6, is the ratio of the actual dynamic pressure to the one-dimensional dynamic pressure $(\frac{q}{\frac{1}{2}\rho\bar{U}^2})$. As the velocity profile becomes more peaked, n decreases and this coefficient will increase. Hence the actual dynamic pressure of the flow, as shown by the velocity profile shape, (Figures 5 and 7) will increase, thereby lowering the static pressure. Only at relatively large values of the radial coordinate $(\frac{r}{d}>3)$ do the differences in static pressure, reflecting the differences in the thickness of the inlet boundary layer, become small.

Figure 10 gives the pressure along the outer boundary 0 - 0 of the inlet bend. It is interesting to note that there is a considerable flattening of the pressure profile when the centre-body is removed. It may be recalled that the flow model from which the boundary shape 0 - 0 was determined is an impinging axisymmetric jet. If this model

4.3 Optimum Bend Design

In order to determine the effects of expanding or contracting the flow in the bend, a study was made of the pressure recovery when the channel width was varied. Figure 11 shows the pressure recovery coefficient C_{p_R} plotted against the channel width for this case, and it is apparent that the optimum $\frac{h}{d}$ value is very close to that for the constant area bend. The reduction in area ratio as the channel width decreases must increase the exit kinetic energy loss, but this effect is quite small within the range of area ratios tested. Therefore, the decrease in pressure recovery below the optimum channel width $\frac{h}{d}$ must be primarily due to increased channel pressure losses, while the decrease above the optimum $\frac{h}{d}$ must be due both directly and indirectly to increased inlet bend losses. It should be noted that at low values of $\frac{h}{d}$, the pressure recovery becomes independent of both the inlet boundary layer thickness and the presence of a centre-body. As $\frac{h}{d}$ becomes quite large, the flow becomes unsteady and highly turbulent.

4.4 Optimum Area Ratio $\frac{A_e}{A_i}$

As the channel diameter is increased, the kinetic energy leaving loss will be reduced. The channel friction pressure losses, however, will increase. Figure 12 shows the pressure recovery for increasing area ratio $\frac{A_e}{A_i}$, as determined from equation (10). It is evident that there is little to be

gained in pressure recovery by designing to the theoretical optimum area ratio as given by equation (11). If the diffuser is to be used to recover the total kinetic energy of the flow, an area ratio of approximately five ($\frac{A_e}{A_i} \approx 5$) would seem to be the practical optimum, since size limitations would usually take priority over performance.

4.5 Off Design Performance

A few experimental studies were made in order to determine the effects of operating the radial diffuser at other than its design configuration. In one experiment, the front and back disc were set at an angle to each other such that the exit channel width was about 40% larger on one side than the other. The pressure recovery was reduced by only 5% with this configuration.

In a second experiment, a very small disturbance was inserted near the channel inlet (0.020 inch hypodermic needle traversing the channel), and this was sufficient to cause the flow to separate from both discs over a large area of the channel, with a resultant inflow of air from the periphery. The pressure recovery in this condition was reduced by more than 15%.

In order to determine whether the screen which was used to reduce the boundary layer thickness was affecting the pressure recovery by altering the turbulence level, a test was carried out using a series of screens which had only a small effect on the shape of the velocity profile but

presumably a large effect on the turbulence. The maximum pressure recovery increased by less than 2%, and this could be accounted for by the slight change in the apparent thickness of the inlet boundary layer. It is concluded, therefore, that inlet turbulence had only a minor effect.

5. CONCLUSIONS

1. The pressure recovery for the radial diffuser may be theoretically predicted with good accuracy for Reynolds numbers $R_d > 2 \times 10^5$ and relatively thin inlet boundary layers. The radial diffuser has a high pressure recovery ($C_{p_R} \approx 0.88$) which is comparable to a 7° conical diffuser ($C_{p_R} \approx 0.90$) under the same entry conditions and at Reynolds numbers which are likely in practical applications ($R_d > 10^5$).

2. An efficient inlet bend from the supply pipe outlet to the radial channel inlet was developed by approximating the experimental free-streamlines for an impinging axisymmetric jet on a flat plate. The maximum pressure recovery occurred with a constant area bend. (Figure 11)

3. The pressure recovery decreases with decreasing Reynolds number for both radial and conical diffusers. However, the decrease is more gradual for the conical diffuser. The pressure recovery for the radial diffuser decreased rapidly for Reynolds numbers below 10^5.

4. The pressure recovery showed a sizeable decrease (approximately 8%) for both radial and conical diffusers when the inlet boundary layer was fully developed ($\delta = \frac{d}{2}$) rather than relatively thin ($\delta < 0.020d$).

5. Installation of a centre-body in the radial diffuser produced very little change in the

pressure recovery. Therefore a centre-body may be used whenever other design considerations make it desirable, e.g., as a housing for a fan motor.

6. For the radial diffuser, a practical optimum area ratio $\frac{A_e}{A_i}$ appears to be approximately five, even though the theoretical optimum ($\frac{A_e}{A_i} = 1.413\ R_d^{1/5}$) is generally much larger.

7. Future work should include the addition of swirl to the flow since the radial diffuser will frequently be used in conjunction with a swirl-producing fan at the inlet section, e.g., in ground effect machines.

6. APPENDIX

The apparatus shown in Figure 13 and 14 was designed to produce swirl-free, incompressible turbulent flow with either a thin ($\delta < 0.02d$) or fully developed ($\delta = \frac{d}{2}$) boundary layer at the inlet to the diffuser. Air was supplied from a centrifugal compressor, driven by a 10 H.P. constant-speed, three-phase motor. The volume flow to the apparatus was roughly controlled by a large bleed valve at the compressor outlet.

The compressor was located approximately 40 feet from the outlet in the research laboratory, and thus the supply pipe was sufficiently long to damp out any large fluctuations in the flow. All the bends in the supply pipe were gradual, and the flow proceeded along a straight run of 12 feet of flexible tubing before passing through a deep-cell honeycomb which helped to eliminate any swirl. It was then contracted at a bleed valve for fine control and passed down a 2 inch diameter tube for another 14 feet before entering the diffuser.

The radial channel was formed by a 0.437 inch thick machined steel back disc, through which the flow entered, and a front disc of 0.375 inch thick plate glass which allowed the use of flow visualization techniques. Two diameters of the disc were used, D = 12 inch. and D = 18 inch. The steel disc was mounted rigidly on a heavy steel framework by three studs, and the glass disc moved on three threaded rods. Three dial

gauges with 0.001 inch graduations were mounted on the rigid frame and rode against the glass disc, so that the channel width could be accurately adjusted. The steel discs were ground within o.ooo5 inch tolerance and then chromium plated. The glass plate was found to be within 0.0001 inch tolerance over its entire surface and proved to be very satisfactory.

All discs were pressure tapped at 0.5 inch radial increments along two alternating azimuthal coordinates, thus providing a continuous check on the angular symmetry; as an additional check, the discs were pressure tapped every 90° at two radial positions. The static pressure taps were 0.015 in. in diameter and were drilled directly into the steel disc. With the glass plate it was first necessary to drill 0.125 inch diameter holes with a carbide tipped drill and then insert brass plugs in which the 0.015 inch diameter tap hole had been drilled; the plugs were glued into place with epoxy resin. To ensure a smooth surface the plugs were mounted slightly proud and hand scraped flush with the glass surface. The inlet pipe was joined to the steel channel wall by the diffuser inlet bend, which was machined from plexiglass and pressure tapped at 0.25 inch increments along its surface in the direction of the flow. The centre-body was also machined from plexiglass and the upstream point rounded to stabilize the stagnation point (see Figure 2).

The conical diffuser was constructed by rolling and welding 0.063 inch thick mild steel sheet. This was joined to the inlet supply pipe outlet by a plexiglass transition section.

To reduce the apparent thickness of the boundary layer at the pipe outlet bronze screens (23 x 24 mesh .011 in. wire diameter and $K \approx 1$) with greater effective porosity near the wall were installed. This was accomplished by super-imposing at 45° a 1.50 inch diameter screen on a 2 inch diameter screen. This composite screen was then mounted near the supply pipe outlet and velocity profile traverses taken in order to determine the effective boundary layer thickness.

The radial diffuser was found to be very sensitive to any disturbance near the channel inlet where the diffusion rate is very high. In order to traverse the flow at the exit of the 90° inlet bend the stem of a 0.020 inch diameter pitot tube was mounted approximately 8 channel widths downstream of the traversing section with its nose extending the required distance upstream. The static pressure at the traversing section was taken as the mean between the wall static pressure on the front and back discs since the variation across the channel was small (less than 2%).

The lower pitot-static pressures, were measured with an accurate reservoir manometer filled with alcohol which could be inclined up to 25:1. Greater pressure differences were measured on a large vertical alcohol manometer. The bend and channel static pressures were measured with a multi-tube alcohol manometer.

REFERENCES

1. Moller P.S. — Radial Flow Without Swirl Between Parallel Discs. Aeronautical Quarterly, Vol.XIV, p.163 (May 1963)

2. Hofmann, A. — Die Energieumsetzung in Saugrohrahn-licherweiterten Dusen. Mitteilungen. Hydraulischen Institut Th. Muchen, Heft 4. (1931)

3. Kline, S.J. Abbott, D.E. and Fox, R.W. — Optimum Design of Straight-Walled Diffusers. Journal of Basic Engineering, p.321. (Sept. 1959)

4. Robertson, J.M. and Ross, D. — Effect of Entrance Conditions in Diffuser Flow. Trans. A.S.C.E., Vol.118, p.1063 - 1097 (1953)

5. McLellan, C.H. and Nichols, M.R. — An Investigation of Diffuser-Resistance Combinations in Duct Systems. NACA ARR L329 (1942)

6. Waitman, B.A. Reneau, L.R. and Kline, S.J. — Effects of Inlet Conditions on Performance of Two-Dimensional Subsonic Diffusers. Journal of Basic Engineering, p.349 (Sept. 1961)

7. Reich, Fr. — Deflection of a Free Liquid Stream on an even Plate at Right-Angle to the Direction of the Flow. Diss. Hannover or VDI-Forsch - Heft 290 (German) (1926)

8. Schacht, W. — Deflection of a Free Liquid Stream on an Even Plate. Diss. Hannover or Ing. Arch.5 p.245 (German) (1934)

9. McLellan, H. and Bartlett, W.A. Jr. — Investigation of Air Flow in Right Angle Elbows in a Rectangular Duct. NACA ARR, (L328) (Oct. 1941)

10. Wirt, L. — New Data for the Designing of Corners in Duct Systems. General Electric Review, Vol.30, No.6 (June 1927)

11. Ito, H. — Friction Factors in Turbulent Flow in a Curved Pipe. Trans. ASME D81, (Journ. of Basic Engineering), p.123 (1959)

12. Weske, J.R. — Pressure Loss in Ducts with Compound Elbows. NACA ARR, (Feb. 1943)

13. Marks, A.W. — Radial Distributions of Temporal-Mean Peripheral Velocity and Pressure for Fully Developed Turbulent Flow in Curved Channels. Trans. ASME, p.528 (Sept. 1960)

14. Schlichting, H. — Boundary Layer Theory. McGraw-Hill, 4th edition, p.537, (1960)

15. Gibson, A.H. — On the Flow of Water Through Pipes and Passages Having Converging or Diverging Boundaries. Proc. Roy. Soc., London, Series A, Vol.83, p.366 - 378. (1910)

IMPINGING AXISYMMETRIC JET
ON A FLAT PLATE

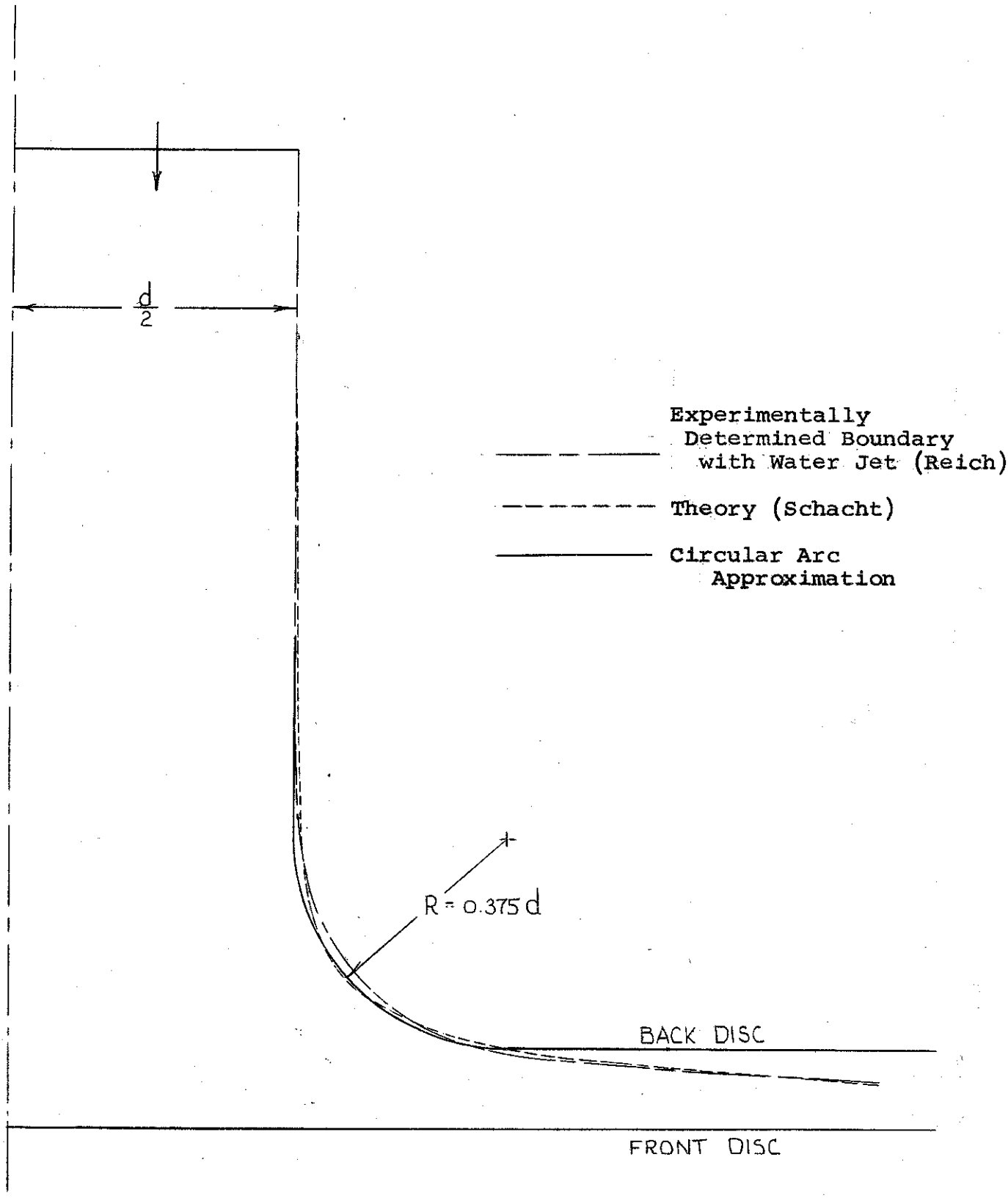

FIGURE 2

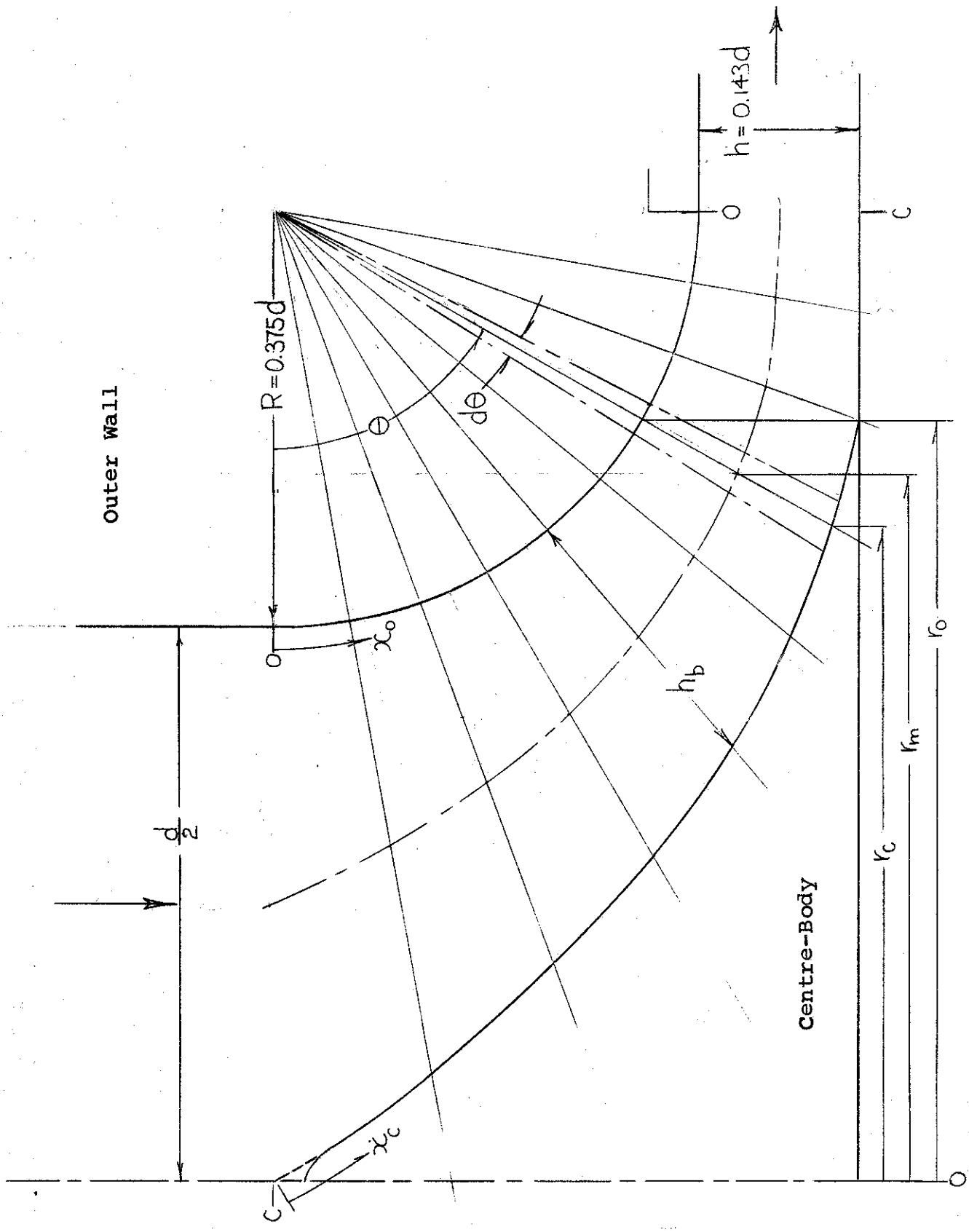
INLET BEND
d = 2 in.
h = 0.143d
O
C
R = 0.375d
θ
dθ
Outer Wall
x_o
h_b
r_o
r_m
r_c
d/2
Centre-Body
x_c
C
O

FIGURE 3

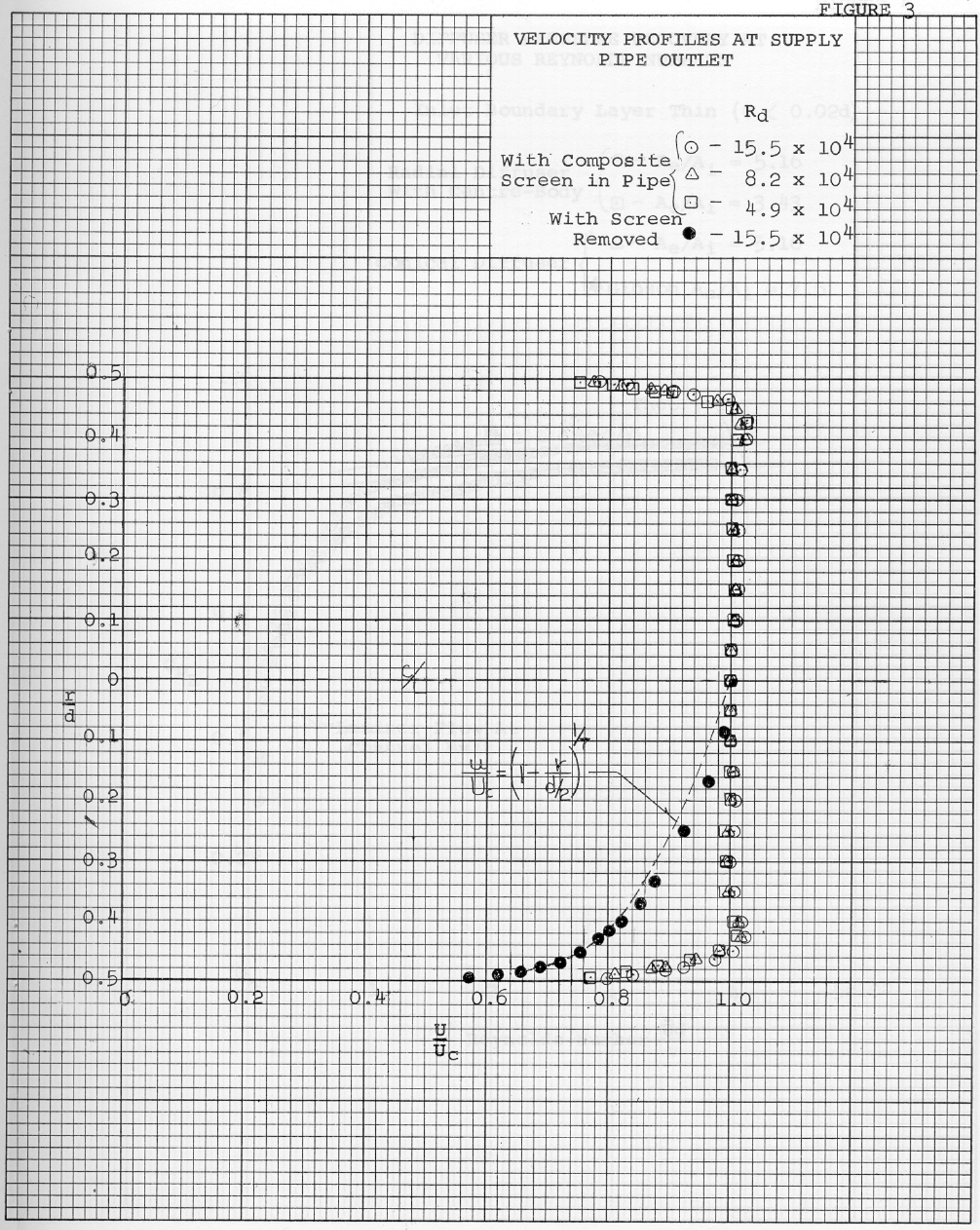
VELOCITY PROFILES AT SUPPLY PIPE OUTLET
R_d
With Composite Screen in Pipe
⊙ - 15.5 x 10^4
△ - 8.2 x 10^4
⊡ - 4.9 x 10^4
With Screen Removed
● - 15.5 x 10^4
0.5
0.4
0.3
0.2
0.1
0
0.1
0.2
0.3
0.4
0.5
r/d
C/L
$\frac{u}{U_c} = \left(1 - \frac{r}{d/2}\right)^{1/7}$
0
0.2
0.4
0.6
0.8
1.0
$\frac{U}{U_c}$

FIGURE 4

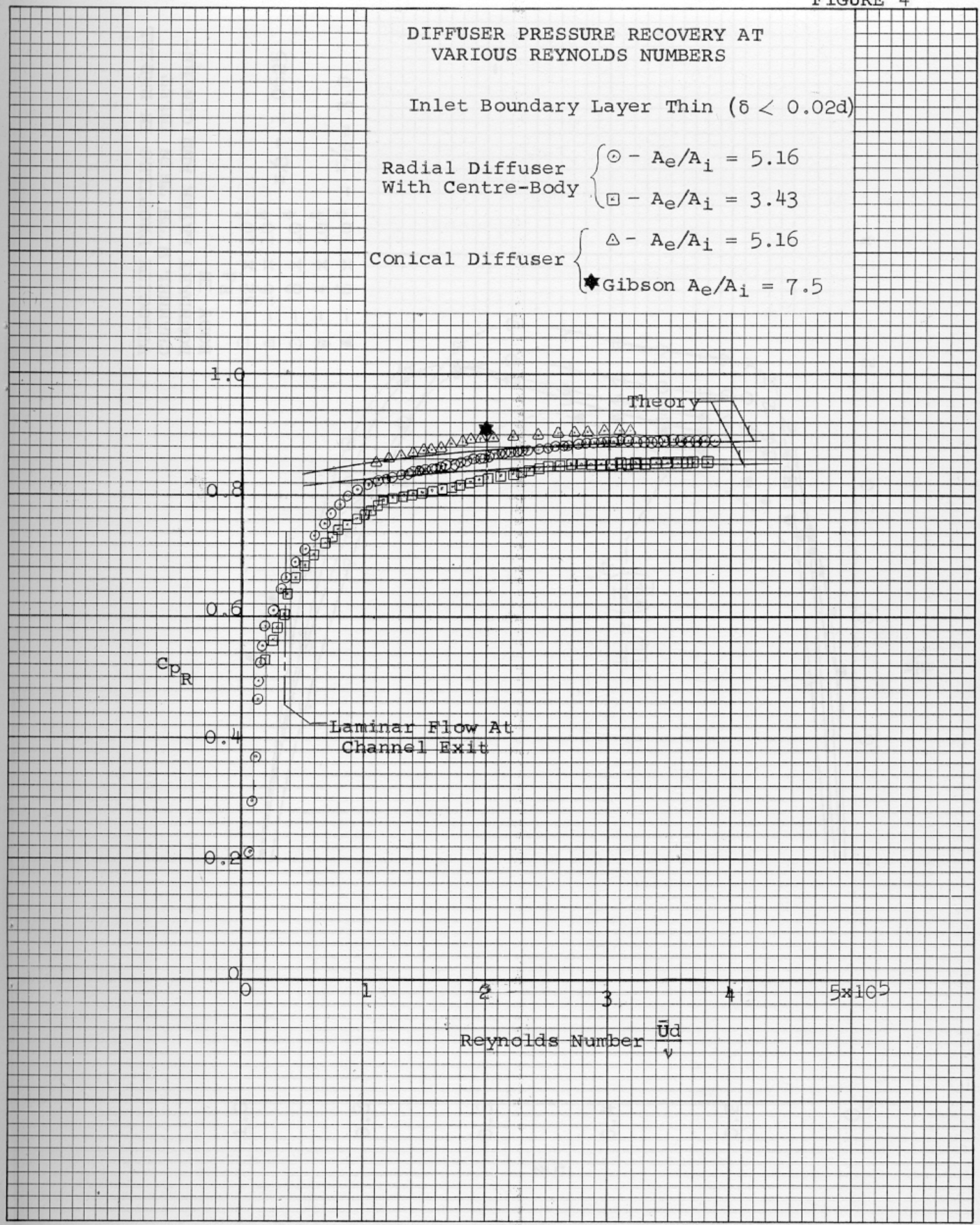
DIFFUSER PRESSURE RECOVERY AT VARIOUS REYNOLDS NUMBERS
Inlet Boundary Layer Thin (δ < 0.02d)
Radial Diffuser With Centre-Body
⊙ - Ae/Ai = 5.16
⊡ - Ae/Ai = 3.43
Conical Diffuser
△ - Ae/Ai = 5.16
Gibson Ae/Ai = 7.5
Theory
Laminar Flow At Channel Exit
Cp_R
1.0
0.8
0.6
0.4
0.2
0
0
1
2
3
4
5x10^5
Reynolds Number Ūd/ν

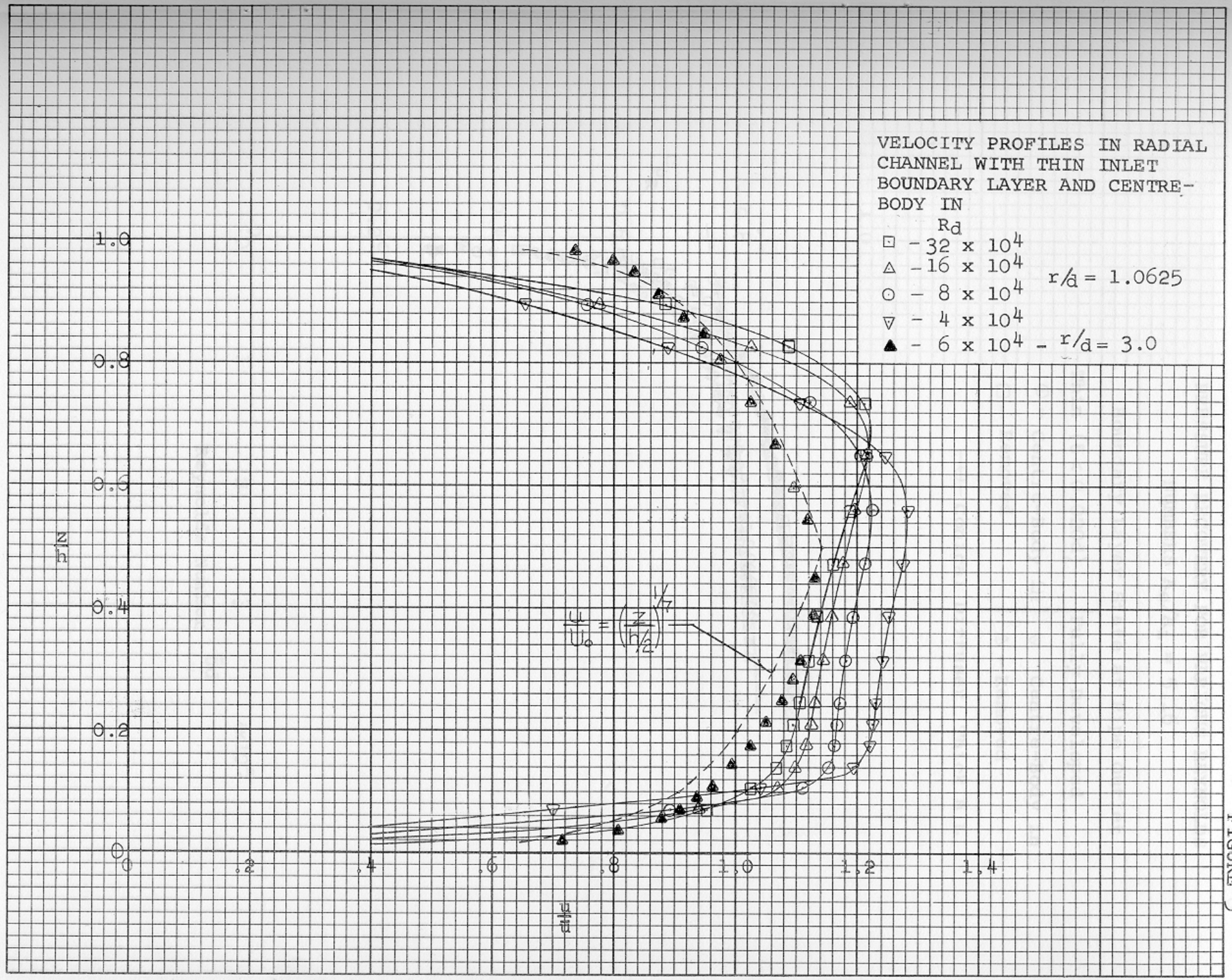
VELOCITY PROFILES IN RADIAL CHANNEL WITH THIN INLET BOUNDARY LAYER AND CENTRE-BODY IN
Rd
□ - 32 x 10^4
△ - 16 x 10^4
○ - 8 x 10^4
▽ - 4 x 10^4
▲ - 6 x 10^4
r/d = 1.0625
r/d = 3.0
u/U0 = (z/h/2)^1/7
z/h
u/U0
1.0
0.8
0.6
0.4
0.2
0.0
.2
.4
.6
.8
1.0
1.2
1.4

FIGURE 5

FIGURE 6

PRESSURE RECOVERY FOR VARIOUS REYNOLDS NUMBERS $A_e/A_i = 5.16$

Boundary Layer State at Pipe Outlet

Thin ($\delta < 0.020d$)	Fully Developed
⊙ – Centre-Body in	▽ – Centre-Body in
⊡ – Removed	△ – Removed

—⊖— Conical Diffuser Thick B.L.

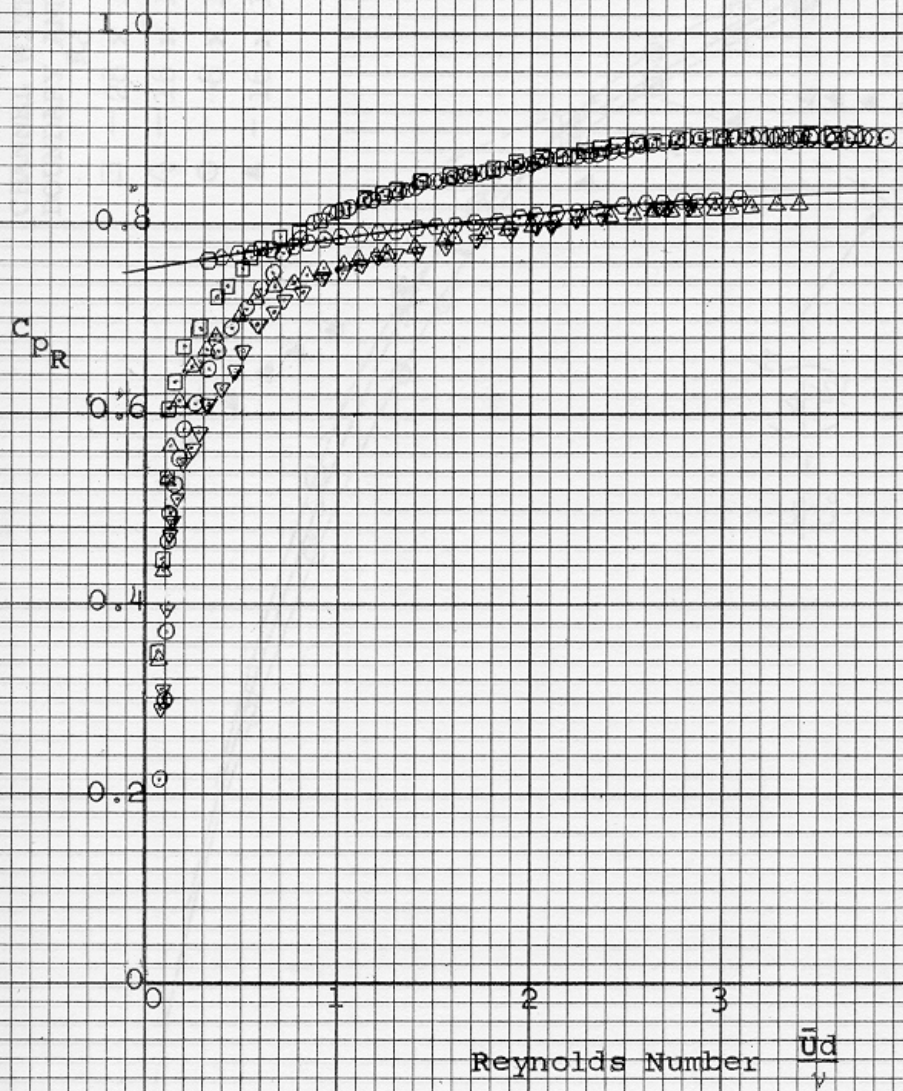

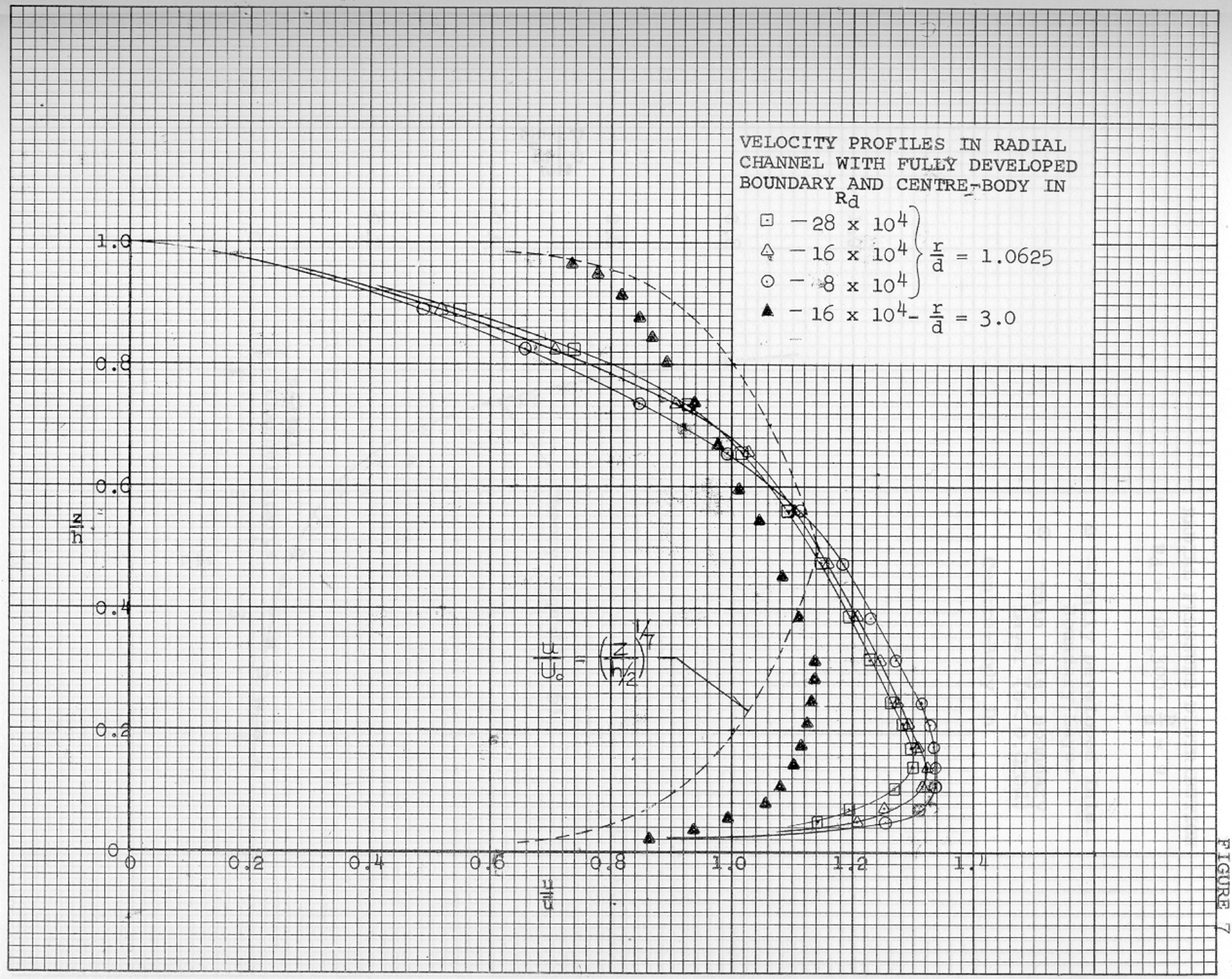
VELOCITY PROFILES IN RADIAL CHANNEL WITH FULLY DEVELOPED BOUNDARY AND CENTRE-BODY IN
R_d
⊡ – 28 x 10^4
△ – 16 x 10^4
⊙ – 8 x 10^4
} $\frac{r}{d}$ = 1.0625
▲ – 16 x 10^4 – $\frac{r}{d}$ = 3.0
$\frac{u}{U_o} = \left(\frac{z}{h/2}\right)^{1/7}$
z/h
u/U
0
0.2
0.4
0.6
0.8
1.0
1.2
1.4

FIGURE 7

FIGURE 8

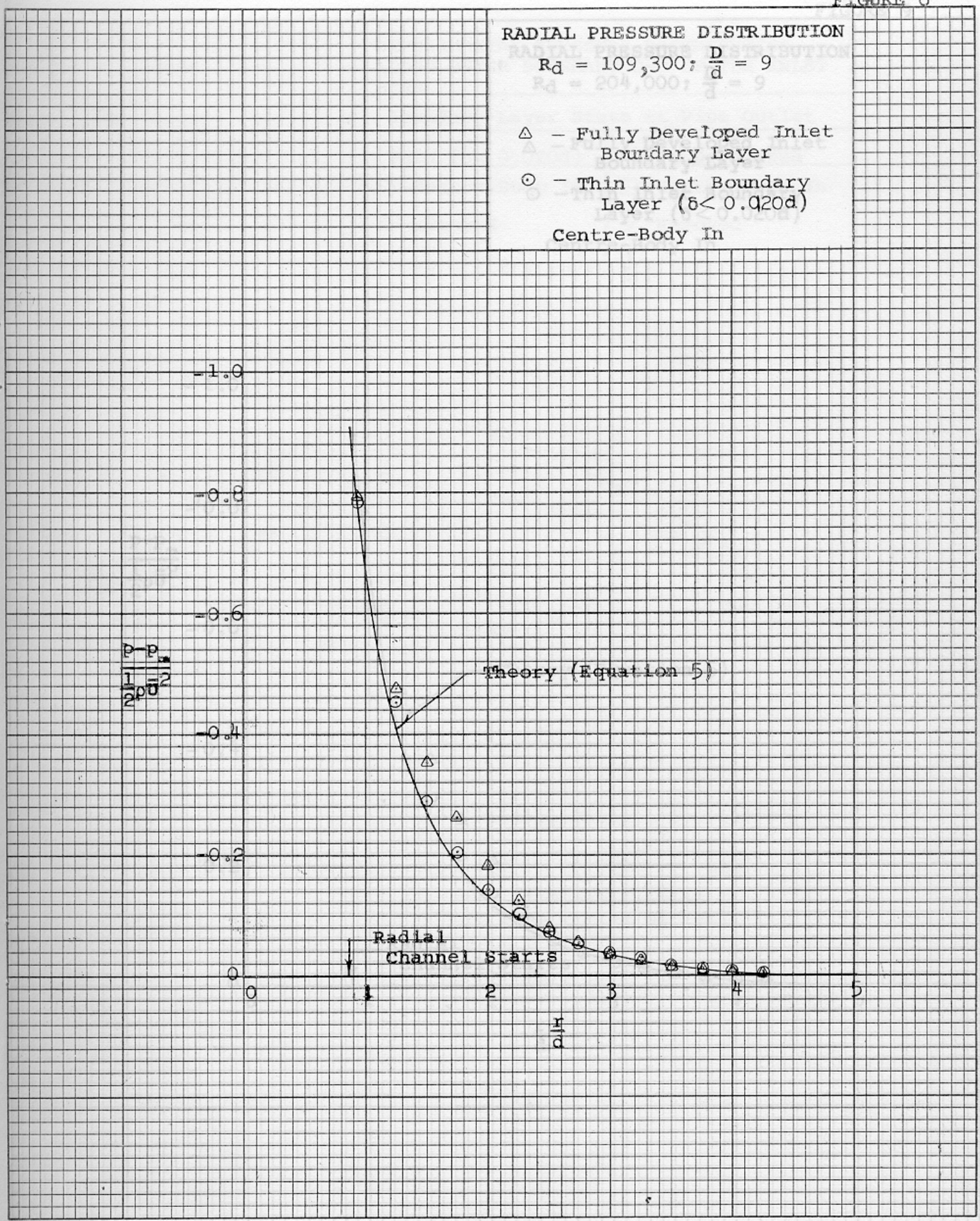
RADIAL PRESSURE DISTRIBUTION
Rd = 109,300; D/d = 9
△ – Fully Developed Inlet Boundary Layer
⊙ – Thin Inlet Boundary Layer (δ< 0.020d)
Centre-Body In
-1.0
-0.8
-0.6
-0.4
-0.2
0
(p-p∞)/(½ρū²)
Theory (Equation 5)
Radial Channel Starts
0
1
2
3
4
5
r/d

FIGURE 9

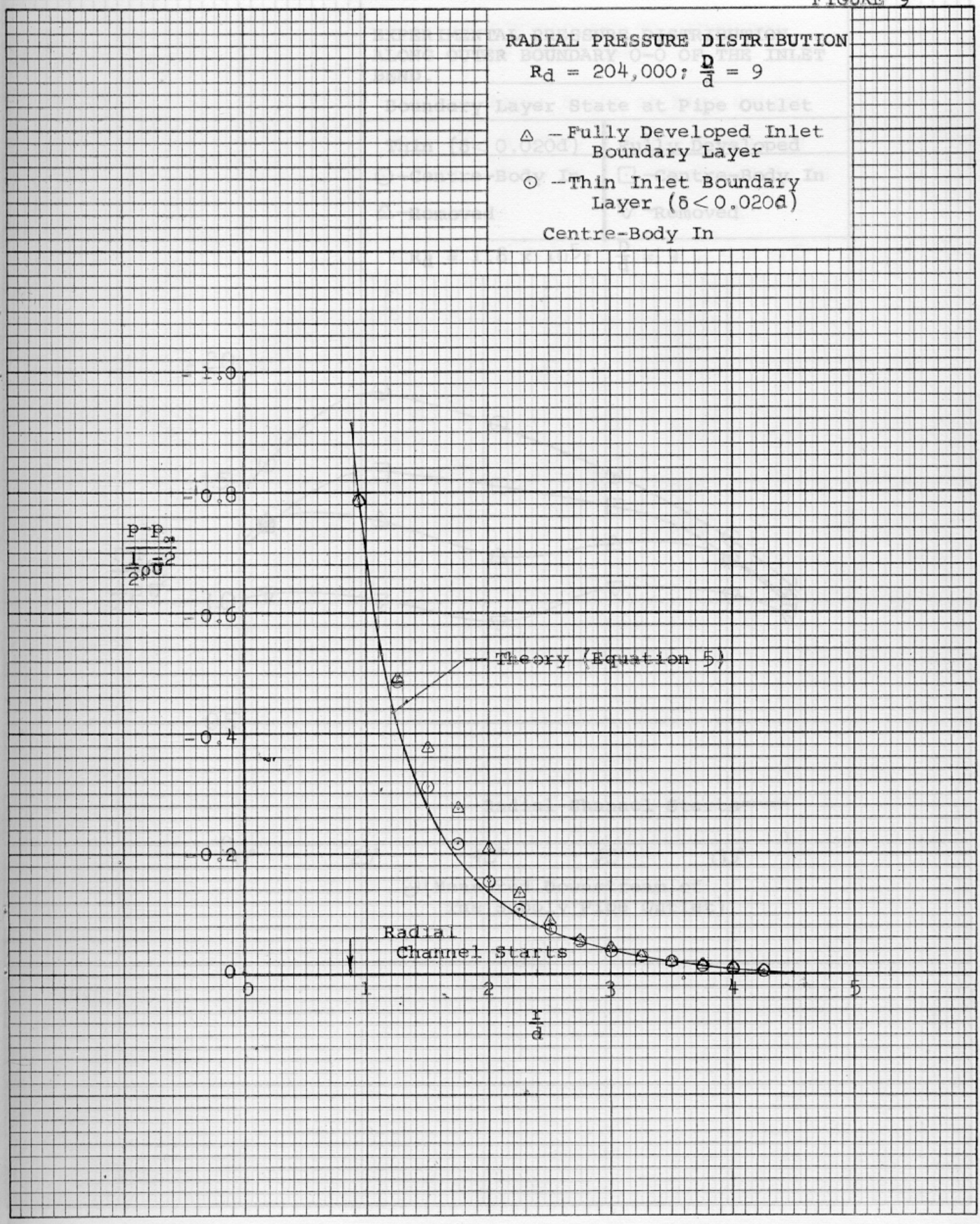
RADIAL PRESSURE DISTRIBUTION
R_d = 204,000; $\frac{D}{d}$ = 9
△ – Fully Developed Inlet Boundary Layer
⊙ – Thin Inlet Boundary Layer (δ < 0.020d)
Centre-Body In
$\frac{p-p_\infty}{\frac{1}{2}\rho\bar{v}^2}$
-1.0
-0.8
-0.6
-0.4
-0.2
0
Theory (Equation 5)
Radial Channel Starts
0
1
2
3
4
5
$\frac{r}{d}$

FIGURE 10

EXPERIMENTAL PRESSURE DISTRIBUTION ALONG OUTER BOUNDARY 0-0 OF THE INLET BEND.

Boundary Layer State at Pipe Outlet

Thin ($\delta < 0.020d$)	Fully Developed
⊙ -Centre-Body In	⊡ -Centre-Body In
△ -Removed	▽ -Removed

$R_d = 1.8 \times 10^5$; $\frac{D}{d} = 9$

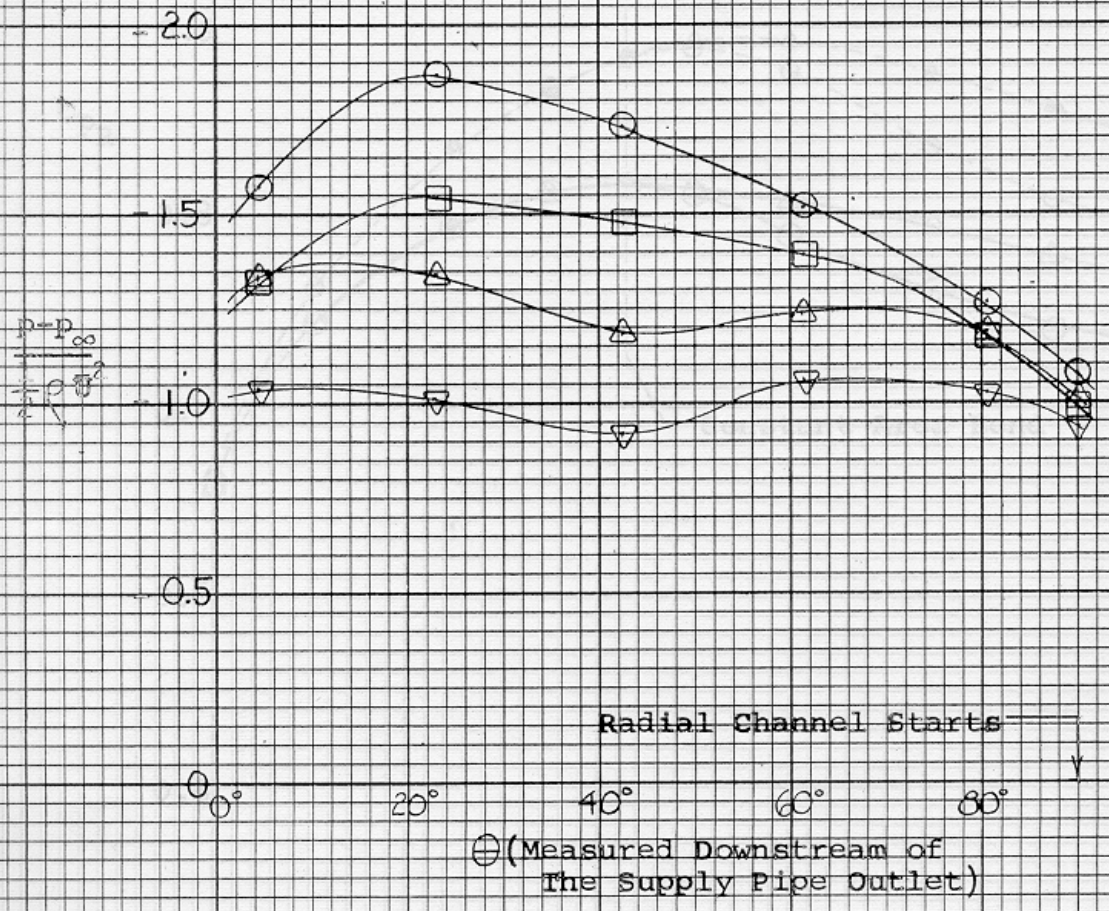

FIGURE 11

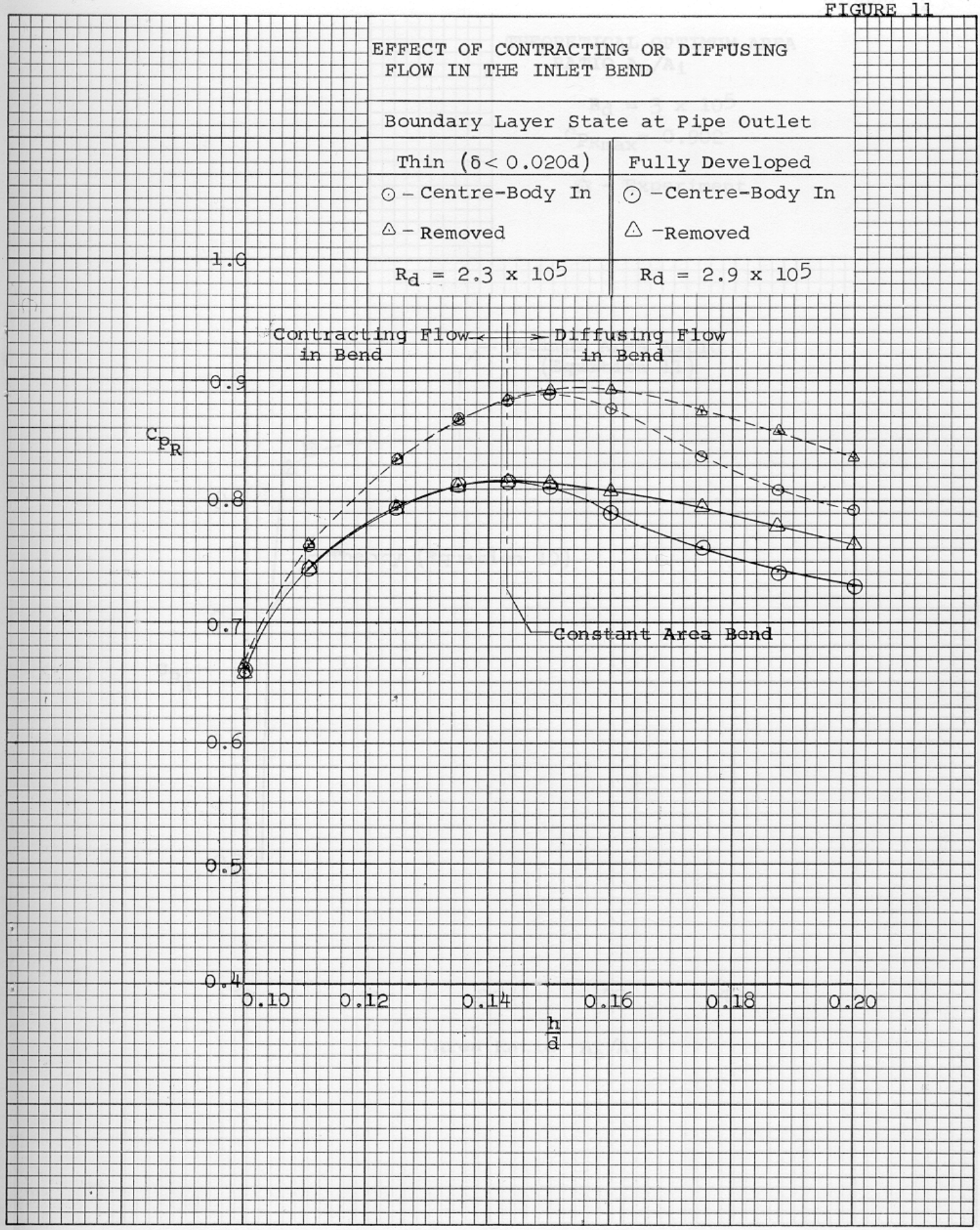
EFFECT OF CONTRACTING OR DIFFUSING FLOW IN THE INLET BEND
Boundary Layer State at Pipe Outlet
Thin (δ < 0.020d)
⊙ – Centre-Body In
△ – Removed
R_d = 2.3 x 10^5
Fully Developed
⊙ – Centre-Body In
△ – Removed
R_d = 2.9 x 10^5
Contracting Flow in Bend
Diffusing Flow in Bend
Constant Area Bend
C_{p_R}
1.0
0.9
0.8
0.7
0.6
0.5
0.4
0.10
0.12
0.14
0.16
0.18
0.20
h/d

FIGURE 12

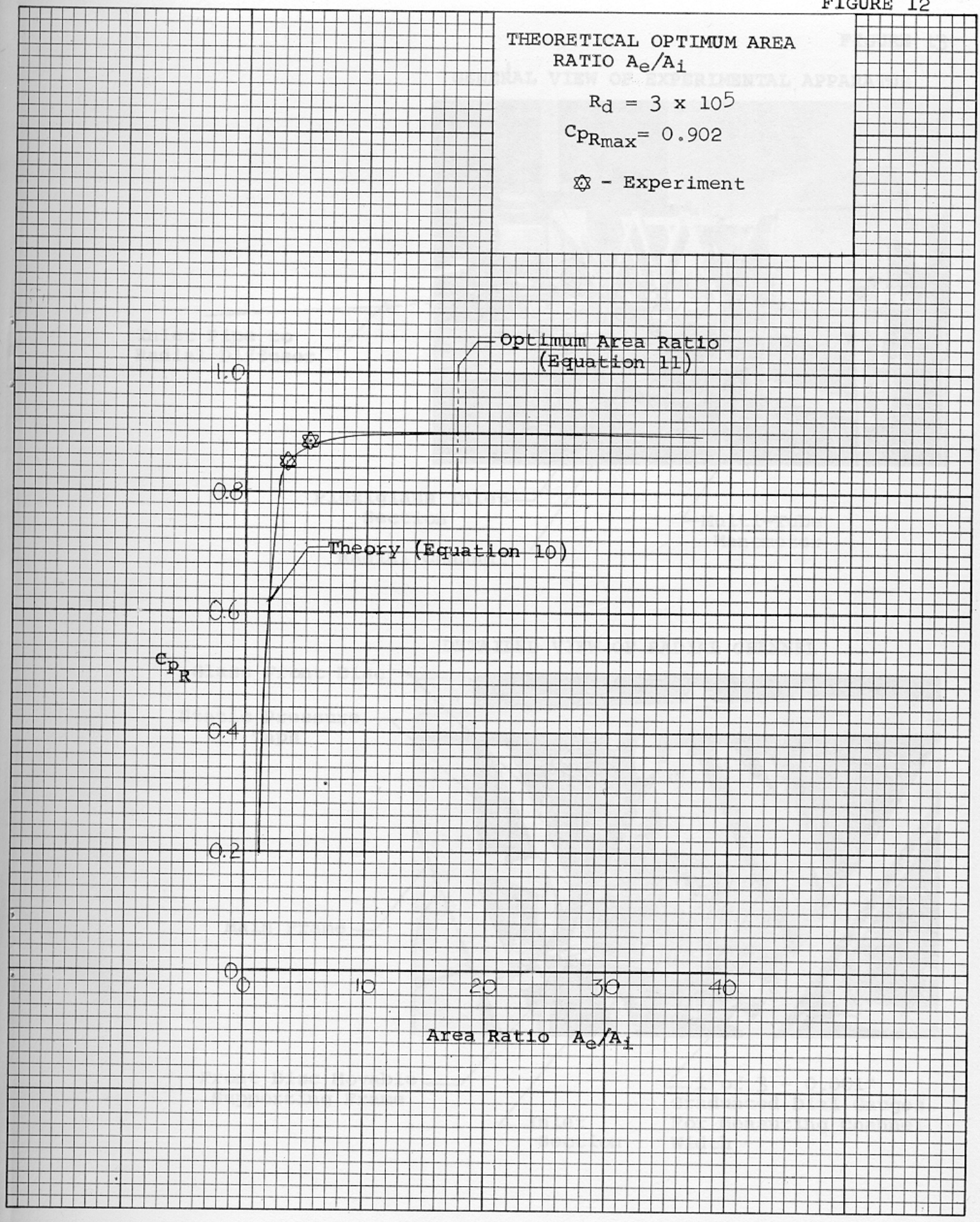
THEORETICAL OPTIMUM AREA RATIO A_e/A_i
$R_d = 3 \times 10^5$
$C_{p_{R_{max}}} = 0.902$
✡ - Experiment
Optimum Area Ratio (Equation 11)
Theory (Equation 10)
C_{p_R}
1.0
0.8
0.6
0.4
0.2
0
0
10
20
30
40
Area Ratio A_e/A_i

FIGURE 13

GENERAL VIEW OF EXPERIMENTAL APPARATUS

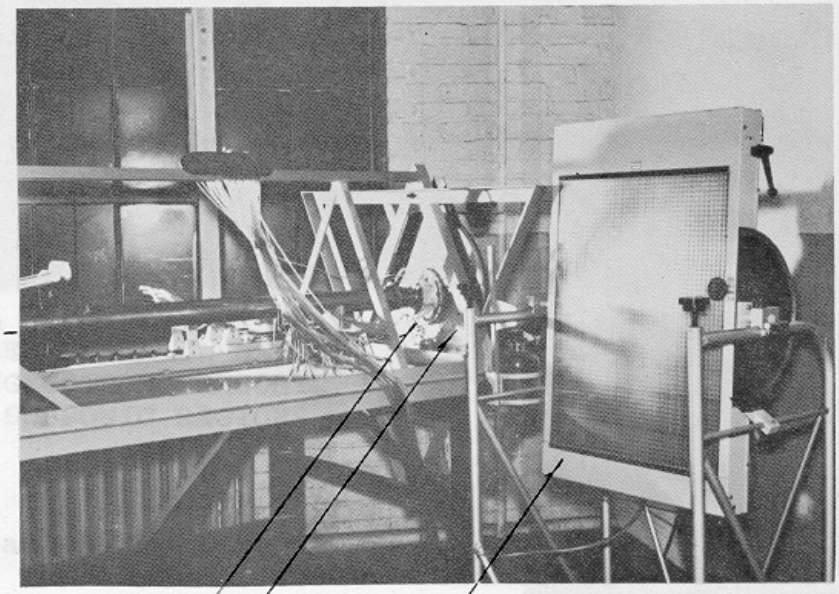

DETAILED VIEW OF RADIAL CHANNEL